Jilin Daxue Xuebao (Gongxueban)/Journal of Jilin University (Engineering and Technology Edition)
ISSN：1671-5497
E-Publication Online Open Access
Vol: 41 Issue: 10-2022
DOI 10.17605/OSF.IO/MH3B9

A COMPARATIVE STUDY OF HIGHLY EFFICIENT A-SI: H/SNS/CDS/ZNS PHOTOVOLTAIC CELLS USING SCAPS-1D

SUTAPA BADYAKAR
currently pursuing Ph.D program in Electrical and Electronics Engineering in BMS College of engineering, Bengaluru, India. E-mail: sutapab@bmsce.ac.in

CHANDASREE DAS
Associate Professor, Department of Electrical and Electronics Engineering in BMS College of engineering, Bengaluru, India.

ABSTRACT:

The computational modelling of a novel photovoltaic cell has showed an enhancement in the empirically validated efficiency of a-Si:H based solar cells. To model and optimize the functionality of the suggested cell, different absorber layer and buffer layer thicknesses are used. The working temperature and illumination is optimized. A key element in enhancing the performance of any photovoltaic device is bandgap grading. Here, the bandgap of the p-type absorber layer is linearly graded. Bulk defects are also added to replicate the optimal structure. Through simulation, the results in V_{oc}, J_{sc}, fill factor, and efficiency of the suggested cell is examined. From 11.62 % to 42.22 %, the optimized cell's efficiency shows a significant rise. The reference model (p-i-n a-Si:H), a-Si:H/CdS, a-Si:H/SnS/CdS, and a-Si:H/SnS/CdS/ZnS (proposed model) are four architectures that are investigated and contrasted. The one with the highest efficiency is a-Si:H/SnS/CdS/ZnS. The SCAPS - 1D solar simulator is used to simulate the project.

INDEX TERMS: a-Si:H, Absorber layer, Bandgap Grading, Buffer Layer, Efficiency, Thickness, Solar Cell

1 INTRODUCTION

Photovoltaic refers to the process of a semiconductor directly converting solar energy into electrical energy. The photovoltaic effect happens when electromagnetic radiation causes a potential difference to form at the intersection of two distinct materials. There are three separate processes that make up the photovoltaic effect [1]. The first step in the process is the absorption of light, which creates charge carriers. The created charge carriers are separated during the second step. The charge carriers are collected at the electrodes as the final step. Due to its abundance and low cost of fabrication, hydrogenated amorphous silicon (a-Si:H) has received significant attention from the major thin film solar cells [2]. Tin sulphide is a photovoltaic cell component that is ample, secure, and advantageous to the environment [3]. Future solar cell panels are anticipated to use this inexpensive material. In this work, a solar cell is constructed and simulated with an a-Si:H and SnS heterojunction absorber layer. One of the most important factors in solar cell's development is the buffer layer, which controls their photovoltaic characteristics. From a physics perspective, the buffer layer affects the overall band structure and provides band alignment between the absorber and window layers [4]. In this work, a-Si:H based photovoltaic solar cells are compared based on a numerical analysis carried out by SCAPS (Solar Capacitance Simulator)

Jilin Daxue Xuebao (Gongxueban)/Journal of Jilin University (Engineering and Technology Edition)
ISSN：1671-5497
E-Publication Online Open Access
Vol: 41 Issue: 10-2022
DOI 10.17605/OSF.IO/MH3B9

software tool, 3.3.10 version [5]. Based on a reference cell, a new photovoltaic cell is proposed by adding p-type absorber layer and n-type buffer layers to the p-layer of the a-Si:H. The cell structure sequences are a-Si:H/CdS, a-Si:H/SnS/CdS, a-Si:H/SnS/CdS/ZnS. The various input parameters for different layers are provided into SCAPS for simulation. The SCAPS-1D software delivers findings on band energy, I-V, C-V, C-f, and quantum efficiency characteristics and accepts inputs such as electrical parameters, optical parameters, and illumination spectrum [6].

2 METHODOLOGY

A reference pin junction solar cell is used [7]. The n-doped, intrinsic, and p-doped silicon layer, as well as the back and front electrodes, make up this basic p-i-n hydrogenated amorphous silicon solar cell. The first process involves photons being absorbed by the materials that make up a junction. A single photon of light that incident on the solar cell is displayed in fig. 1(a). A pair of electrons and holes are produced upon photon absorption. A positively charged hole is left behind when a negatively charged electron is accelerated to a higher energy state. Here, one photon of light is activating a single electron hole pair, but in reality, a whole spectrum of light will generate numerous electron hole pairs at once. The lifetime of the electron hole pair is finite, and eventually recombination may take place. Consequently, the electron will return to its original condition. If this occurs, that absorbed energy is essentially wasted and cannot be turned into electrical energy. Therefore, these charge carriers must be separated in order to actually generate power. In a solar cell, after carriers are created, they begin to move due to a variety of factors, including drift, random motion, and diffusion. Semi-permeable membranes are placed on both sides of the absorber in order to segregate the photo-generated charge carriers. This makes sure that holes can only exit via one membrane and that electrons can only exit through the other. Charges are produced in the p-type semiconductor in the reference cell in this instance. Only electrons and holes are permitted to flow through the solar cell's junctions, which are located at its top and bottom, respectively. Therefore, it is necessary to build the solar cell so that the mobile charge carriers finally encounter those obstacles and separate. Charge carriers are now being produced and separated. The collecting of the charge carriers produced by photo-generation is the last step in the process. Many different charge carriers are produced and separated under the effect of light. There is a potential differential between the electrodes due to the different charge carrier densities at the device's two ends. The term open circuit voltage (v_{oc}) refers to this potential. If a circuit is provided externally between these electrodes, electrons will go from the n-type material to the p-type material. In light of this, the definition of electrical power is the straight flow from a high potential to a low potential. Charge carriers are removed from solar cells in this manner. Once the electrons and holes have completed the circuit and are recombining at the metal absorber interface, the chemical energy of the electron-hole pair is now transformed to electric energy. The efficiency of the reference cell, an amorphous hydrogenated p-i-n junction silicon cell, is 11.62 %. Three further structures are created based on this.

Jilin Daxue Xuebao (Gongxueban)/Journal of Jilin University (Engineering and Technology Edition)
ISSN：1671-5497
E-Publication Online Open Access
Vol: 41 Issue: 10-2022
DOI 10.17605/OSF.IO/MH3B9

As shown in fig. 1(b), the reference cell is altered by including an additional n-type CdS buffer layer on top of the pre-existing p-type a-Si:H layer. Then, as illustrated in fig. 1(c), an additional p-type SnS absorber layer is added to the cell to boost efficiency. The final proposed new solar cell is formed by adding an n-type ZnS to the cell structure since ZnS has a very high refractive index and is also employed as an anti-reflection coating, as illustrated in fig. 1(d). For all simulations, the front and back contacts are maintained as flat bands. All four structure's electrical properties have been researched.

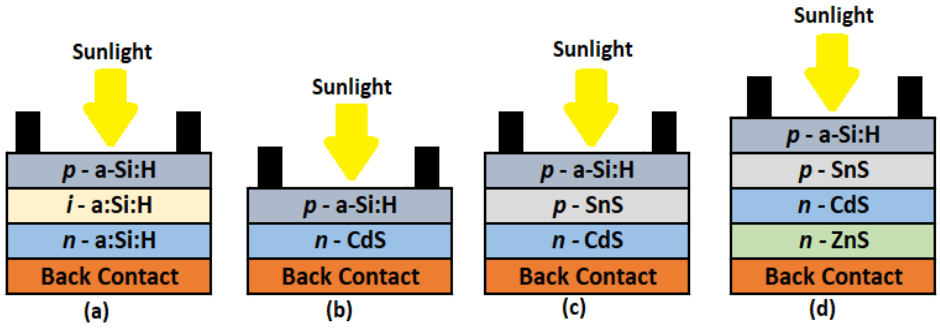

Fig. 1: (a) *p-i-n* a-Si:H (b) a-Si:H/CdS (c) a-Si:H/SnS/CdS (d) a-Si:H/SnS/CdS/ZnS

There are three input panels in the simulation tool SCAPS-1D: the action panel, where the working conditions and expected characteristic outcomes are set; the solar cell definition panel, where the solar cell structure is defined; and the layer property panel, where the electrical and optical properties of the layer material are defined. The SCAPS-1D tool is used to change the bandgap, apply bandgap grading, change the working temperature, change the defects and illumination inputs, and change the thicknesses of the absorber layer and buffer layer [8]. The input electrical parameters for the SCAPS tool is given in table 1 [9], [10, [11], [12].

Jilin Daxue Xuebao (Gongxueban)/Journal of Jilin University (Engineering and Technology Edition)
ISSN：1671-5497
E-Publication Online Open Access
Vol: 41 Issue: 10-2022
DOI 10.17605/OSF.IO/MH3B9

TABLE 1: INPUT ELECTRICAL PARAMETERS FOR THE SCAPS TOOL

Input Parameters	*a-Si:H [9]*	*SnS [10]*	*CdS [11]*	*ZnS [12]*
Thickness (μm)	varied	varied	varied	varied
Band gap (eV)	1.8	1.4	2.45	3.5
Electron affinity (eV)	3.9	4	4.45	4.5
Dielectric permittivity (relative)	11.9	10	10	10
CB effective density of states (cm^{-3})	1E+20	1.18E+18	2.2E+18	1.8E+18
VB effective density of states (cm^{-3})	1E+20	4.76E+19	1.8E+18	1.8E+19
Electron thermal velocity (cm/s)	1E+7	1E+7	1E+7	1E+7
Hole thermal velocity (cm/s)	1E+7	1E+7	1E+7	1E+7
Electron mobility ($cm^2 V^{-1} s^{-1}$)	2E+2	2E+2	1E+2	2E+2
Hole mobility ($cm^2 V^{-1} s^{-1}$)	5E+1	2.5E+1	2.5E+1	2.5E+1
Shallow uniform donor density (cm^{-3})	1E+17	1E+17	1E+18	1E+18
Shallow uniform acceptor density (cm^{-3})	1E+19	1E+19	1E+1	1E+1

3 SIMULATION OUTPUT AND DISCUSSION

3.1 Comparing the four structures on electrical parameters

The thicknesses of the p, i and n layers in the simulated reference cell are 9 nm, 500 nm, and 20 nm, respectively. For the other three structures, the buffer layers of CdS and ZnS are 100 nm thick, while a-Si:H and SnS are 500 nm thick. The working temperature is maintained at 300 K. Illumination spectrum for light source is 1000 W/m^2. The simulation results are shown in table 2.

TABLE 2*:* SIMULATION OUTPUT FOR ALL THE CELLS

Structure	V_{oc} *(V)*	J_{sc} *(mA/cm²)*	*FF (%)*	*η (%)*
p-i-n a-Si:H (Reference Cell)	0.97	17.39	69.15	11.62
a-Si:H/CdS	1.32	12.21	83.24	13.38
a-Si:H/SnS/CdS	1.34	29.08	85.96	33.44
a-Si:H/SnS/CdS/ZnS (Proposed New Cell)	**1.34**	**29.47**	**90.61**	**35.78**

It has been found that as absorber layers and buffer layers are gradually added to the reference cell to design the proposed cell, the V_{oc}, short circuit current (J_{sc}), fill factor (FF), and efficiency (η) all rise. The I-V characteristic curve, as shown in fig. 2, demonstrates that, in comparison to the other three cells, the suggested cell has the largest area under the curve. It follows that the fill factor is at its peak, which results in a higher conversion efficiency of 35.78 %.

Jilin Daxue Xuebao (Gongxueban)/Journal of Jilin University (Engineering and Technology Edition)
ISSN：1671-5497
E-Publication Online Open Access
Vol: 41 Issue: 10-2022
DOI 10.17605/OSF.IO/MH3B9

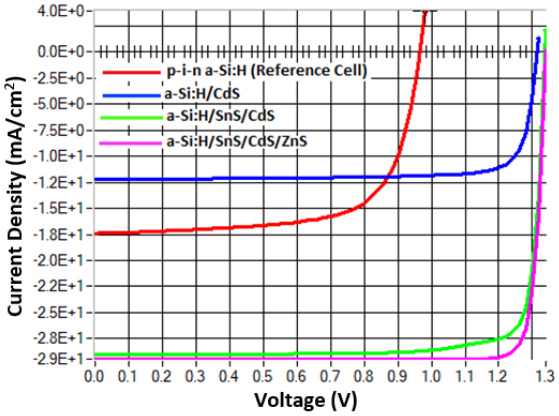

Fig. 2: Current Density - Voltage Characteristic curves of all the four cells

As it is already shown that the proposed cell is giving the highest efficiency among the four structures, next all simulations will be done to improve the proposed cell conversion efficiency.

3.2 Thickness Variation in Absorber Layer and Buffer Layer

In this section the proposed cell (a-Si:H/SnS/CdS/ZnS) is now being optimised for material layer thickness values. The absorber layer and buffer layer thicknesses range from 100 nm to 1000 nm. At 300 K, the operating temperature is maintained. Light source illumination spectrum is 1000 W/m^2. The SnS, CdS, and ZnS layer thicknesses for the first simulation, in which the a-Si:H layer thickness is changed from 100 nm to 1000 nm, are maintained at 500 nm, 100 nm, and 100 nm, respectively. In the second simulation, the a-Si:H, CdS, and ZnS layer thicknesses are maintained at 500 nm, 100 nm, and 100 nm, respectively, while the SnS layer thickness is adjusted from 100 nm to 1000 nm. In the third simulation, the a-Si:H, SnS, and ZnS layer thicknesses are maintained at 500 nm, 500 nm, and 100 nm, respectively. The CdS layer thickness is adjusted from 100 nm to 1000 nm in this simulation. The ZnS layer thickness is adjusted in the fourth simulation from 100 nm to 1000 nm, but the a-Si:H, SnS, and CdS layer thicknesses are maintained at 500 nm, 500 nm, and 100 nm, respectively. In fig. 3, the findings of efficiency versus single layer thickness variation are displayed. As it is observed, the effectiveness of both absorber layers grows as their thicknesses do as well. However, the efficiency of the buffer layer decreases slightly even as its thickness rises.

Jilin Daxue Xuebao (Gongxueban)/Journal of Jilin University (Engineering and Technology Edition)
ISSN：1671-5497
E-Publication Online Open Access
Vol: 41 Issue: 10-2022
DOI 10.17605/OSF.IO/MH3B9

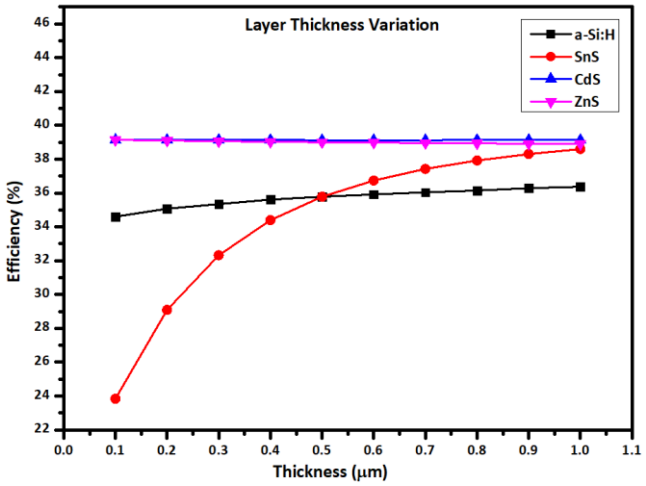

Fig. 3: Conversion Efficiency Vs Layer Width Variation

Next, a simulation is performed to fix the width of the absorber layers. The a-Si:H and SnS layer thicknesses are both variable, ranging from 100 nm to 1000 nm. Each buffer layer's thickness is maintained at 100 nm. Table 3 displays the results. When both of the absorber layers are 1000 nm thick, the cell is seen to reach its maximum efficiency of 39.13 % with the highest V_{oc}, J_{sc}, and fill factor of 1.36 V, 31.75 mA/cm^2 and 90.73 % respectively. As a result, for the remaining of the simulation, the thickness of the a-Si:H and SnS layers is set at 1000 nm for each.

TABLE 3: OUTPUT ELECTRICAL PARAMETERS FOR THE ABSORBER LAYER THICKNESS VARIATION

a-Si:H Thickness (nm)	*SnS Thickness (nm)*	*V_{oc} (V)*	*J_{sc} (mA/cm^2)*	*FF (%)*	*η (%)*
100	100	1.29	17.07	90.43	19.93
100	550	1.31	29.79	90.40	35.16
100	1000	1.31	31.74	90.40	37.51
550	100	1.33	20.00	90.66	24.14
550	550	1.34	29.90	90.61	36.37
550	1000	1.34	31.75	90.62	38.66
1000	100	1.35	21.04	90.63	25.70
1000	550	1.36	29.95	90.75	36.87
1000	**1000**	**1.36**	**31.75**	**90.73**	**39.13**

After that, a simulation is run to fix the buffer layer thickness. The thickness of the CdS and ZnS layers can vary and range from 100 nm to 1000 nm. The thickness of each absorber layer is held constant at 1000 nm. The findings are shown in Table 4. The cell is observed to reach its maximum efficiency of 39.13 % at 100 nm thick buffer layers, with the highest V_{oc}, J_{sc}, and fill factor of 1.36 V, 31.75 mA/cm^2, and 90.73 %, respectively. As a result, the thickness of the CdS and ZnS layers is set to 100 nm for each for the rest of the simulation.

Jilin Daxue Xuebao (Gongxueban)/Journal of Jilin University (Engineering and Technology Edition)
ISSN：1671-5497
E-Publication Online Open Access
Vol: 41 Issue: 10-2022
DOI 10.17605/OSF.IO/MH3B9

TABLE 4: OUTPUT ELECTRICAL PARAMETERS FOR THE BUFFER LAYER THICKNESS VARIATION

CdS Thickness (nm)	*ZnS Thickness (nm)*	*V_{oc} (V)*	*J_{sc} (mA/cm^2)*	*FF (%)*	*η (%)*
100	**100**	**1.36**	**31.75**	**90.73**	**39.13**
100	550	1.36	31.63	90.73	38.99
100	1000	1.36	31.56	90.73	38.90
550	100	1.36	31.75	90.73	39.13
550	550	1.36	31.63	90.73	38.98
550	1000	1.36	31.56	90.73	38.89
1000	100	1.36	31.75	90.73	39.13
1000	550	1.36	31.63	90.73	38.98
1000	1000	1.36	31.56	90.73	38.89

3.3 Working Temperature Variation

The working temperature has a significant impact on the effectiveness of the solar cell. The operating temperature's impact on the suggested cell is shown in this section. As the optimum cell is fixed, the absorber layers and buffer layers each have a thickness of 1000 nm and 100 nm respectively. A 1000 W/m^2 simulation of solar spectrum light is used. Fig. 4. demonstrates the proposed cell's electrical output parameters when the operating temperature is raised from 250 K to 350 K. V_{oc} is shown to gradually fall as the temperature rises. However, as the temperature rises, the J_{sc} rises. As the operating temperature rises, so do the fill factor and efficiency. Therefore, the working temperature is selected, such as at the junction of the V_{oc} and J_{sc} curves, in order to determine the best working state. 300 K is the point. Therefore, the operating temperature is maintained around 300 K to further optimize it for realistic real-time scenarios.

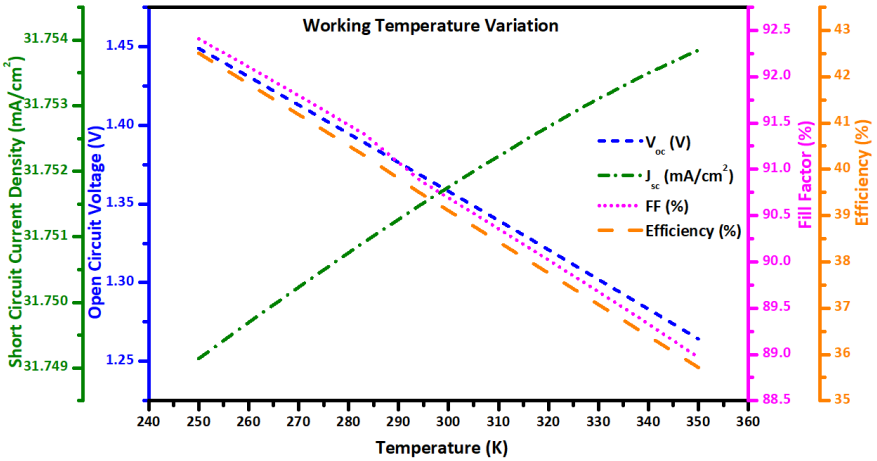

Fig. 4: Electrical output of a-Si:H/SnS/CdS/ZnS with Working Temperature Variation

Jilin Daxue Xuebao (Gongxueban)/Journal of Jilin University (Engineering and Technology Edition)
ISSN：1671-5497
E-Publication Online Open Access
Vol: 41 Issue: 10-2022
DOI 10.17605/OSF.IO/MH3B9

3.4 Illumination Variation

The SCAPS tool has a setting that allows illumination to come from either the p or n side of the solar cell. In fig. 5(a), the cell is shown lit from the p-side, with the first layer being 1000 nm thick a-Si:H, the second layer being 1000 nm of SnS, and the third and fourth levels being 100 nm thick n-type buffer layers. The left front contact illuminates the cell while the right contact is grounded. The cell is lighted from the n-side, as shown in Fig. 5(b), where the first layer is 100 nm thick ZnS, the second layer is 100 nm thick CdS, and the third and fourth layers are p-type absorber layers, each of which is 1000 nm in thickness. The cell is lighted from the right contact, which is also grounded.

Fig. 5(a): a-Si:H/SnS/CdS/ZnS structure with p-side Illumination

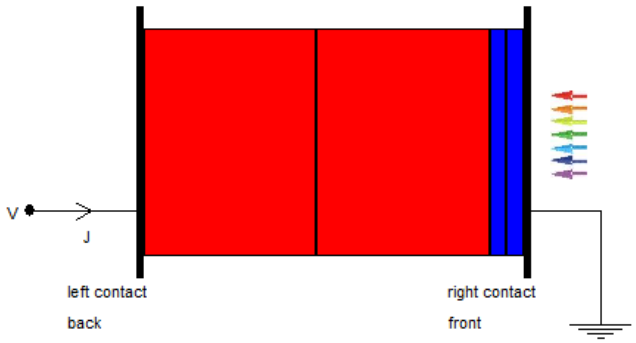

Fig. 5(b): a-Si:H/SnS/CdS/ZnS structure with n-side illumination

The goal of this simulation is to improve the cell's functional structure. Table 5 makes it abundantly evident that the efficiency is significantly higher when the cell is illuminated from the n-side than when it is illuminated from the p-side. Therefore, the solar spectrum should fall on the n-side when the actual cell is depicted. As can be seen, when light from the p-side, the absorber layer width is greater, which results in a longer time needed to reach the junction and a slower rate of recombination. Before the photons can form an electron hole pair and contribute to current generation, they are absorbed and discarded before they reach the junction.

Jilin Daxue Xuebao (Gongxueban)/Journal of Jilin University (Engineering and Technology Edition)
ISSN：1671-5497
E-Publication Online Open Access
Vol: 41 Issue: 10-2022
DOI 10.17605/OSF.IO/MH3B9

TABLE 5: OUTPUT ELECTRICAL PARAMETERS FOR THE ILLUMINATION SIDE VARIATION

Illumination	V_{oc} (V)	J_{sc} (mA/cm²)	FF (%)	η (%)
p-side	1.34	17.80	90.62	21.67
n-side	1.36	31.75	90.73	39.13

3.5 Bandgap Grading

It is possible to increase efficiency using bandgap grading over 32 % using SCAPS. Bandgap grading is one crucial factor to consider while attempting to maximize any device's efficiency. One layer at a time, the p-type materials are graded. A linear grading system is used. The simulations in table 6 are done using a-Si:H and SnS layer combinations with positive and negative grading. When the bandgap varies from 1.8 eV to 1.2 eV, a-Si:H is graded positively. When the bandgap is changed from 1.2 eV to 1.8 eV, a-Si:H is graded negatively. When a-Si:H bandgap grading is not used, the bandgap is fixed at 1.8 eV. When the bandgap varies from 1.4 eV to 1.2 eV, SnS is graded positively. SnS grades negatively when the bandgap varies from 1.2 eV to 1.4 eV. When SnS bandgap grading is not used, bandgap is fixed at 1.4 eV. When neither of the two layers are graded, the efficiency, according to the research, is 39.13 %. In this situation, the fermi level energy of the p side (F_p) coincides with the energy of the conduction band (E_c), as shown in Fig. 6(a). The lowest efficiency among all the combinations is 34.70 % when the SnS bandgap is ungraded while the a-Si:H bandgap is negatively graded from 1.8 eV to 1.2 eV at a composition of 0.9. Since the conduction band energy is significantly higher than the fermi level energy in the case of an a-Si:H negative grading, Fig. 6(b) shows the energy band diagram for the efficiency with the lowest level. The highest efficiency of 44.89 % among all the combinations is realized when the a-Si:H bandgap is ungraded but the SnS bandgap is negatively graded from 1.2 eV to 1.4 eV at a composition of 0.9, as shown in Fig. 6(c), where the conduction band energy falls below the fermi level energy.

TABLE 6*:* OUTPUT PARAMETERS FOR BANDGAP GRADING

Bandgap (a-Si:H)	*Bandgap (SnS)*	V_{oc} (V)	J_{sc} (mA/cm²)	FF (%)	η (%)
Positive Grading	Without Grading	1.30	33.12	90.39	38.88
Positive Grading	Positive Grading	1.30	35.66	90.38	41.92
Positive Grading	Negative Grading	1.30	36.59	90.38	43.03
Negative Grading	Negative Grading	1.22	36.33	89.88	39.79
Negative Grading	Positive Grading	1.22	35.34	89.88	38.73
Negative Grading	Without Grading	1.22	31.74	89.89	34.70
Without Grading	Positive Grading	1.36	35.35	90.72	43.65
Without Grading	**Negative Grading**	**1.36**	**36.34**	**90.72**	**44.89**
Without Grading	Without Grading	1.36	31.75	90.73	39.13

Jilin Daxue Xuebao (Gongxueban)/Journal of Jilin University (Engineering and Technology Edition)
ISSN：1671-5497
E-Publication Online Open Access
Vol: 41 Issue: 10-2022
DOI 10.17605/OSF.IO/MH3B9

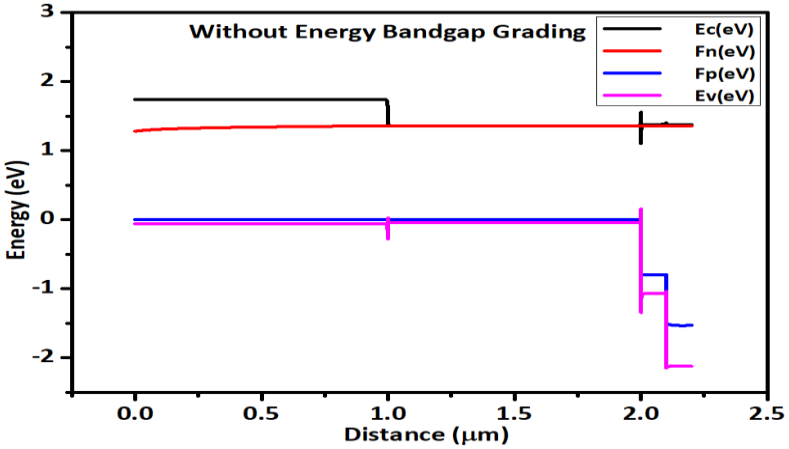

Fig. 6(a): Energy Bandgap Diagram Without bandgap grading

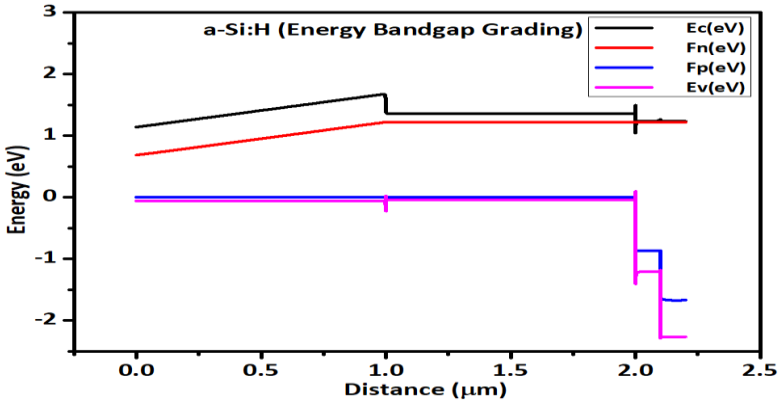

Fig. 6(b): Energy Bandgap Diagram with negative bandgap grading of a-Si:H layer

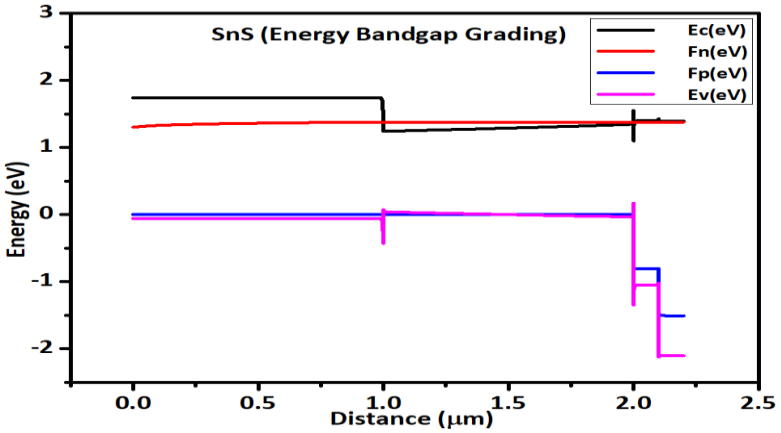

Fig. 6(c): Energy Bandgap Diagram with negative bandgap grading of SnS layer

Jilin Daxue Xuebao (Gongxueban)/Journal of Jilin University (Engineering and Technology Edition)
ISSN：1671-5497
E-Publication Online Open Access
Vol: 41 Issue: 10-2022
DOI 10.17605/OSF.IO/MH3B9

3.6 Defects Variation

This simulation analysis can provide some understanding of the device defects and their impact on efficiency. In a situation when genuine defects result in lower efficiencies. As a result, a few defects are added to the optimized structure in consideration of that. The a-Si:H absorber layer now has two defects. Amphoteric type is the first defect. Grading and overall density are both consistent. The distribution of energy is a Gaussian distribution. Below the conduction band is the reference point for the defective energy level. The energy of the characteristic is 0.288 eV, whereas the energy of the correlation is 0.200 eV. The cross sections for capturing electrons and holes are $3e^{-15}$ cm^2 and $3e^{-14}$ cm^2, respectively. The second defect is an acceptor with a homogeneous overall density and grading. Conduction band tail type energy distribution. Hole and electron capture cross sections are both $1e^{-19}$ cm^2, respectively. The efficiency along with V_{oc}, J_{sc}, and fill factor decreases after simulation with defects. However, it is always preferable to include certain defects. Accordingly, in this improved final proposed cell defects are included and reported as indicated in table 7. The final efficiency is 42.22 %.

TABLE 7: OUTPUT ELECTRICAL PARAMETERS FOR DEFECTS VARIATION

Defects	V_{oc} *(V)*	J_{sc} *(mA/cm²)*	*FF (%)*	*η (%)*
With Defects (a-Si:H)	1.33	36.33	87.63	42.22
Without Defects	1.36	36.34	90.72	44.89

4 Comparative analysis: Reference Cell and Optimized Cell

The last comparison is between the improved suggested cell and the initial reference cell. After adding an additional absorber and buffer layer to the reference cell, the electrical characteristic findings demonstrate the very high efficiency of the new suggested cell. The outputs for V_{oc}, J_{sc}, fill factor, and efficiency are shown in Table 8. According to studies on quantum efficiency (QE), as seen in fig. 7(a), the quantum efficiency increases when the wavelength of the incident light is increased. While for the reference cell, the QE rises from 80 % to 90 % when wavelength increases from 300 nm to 350 nm, then progressively falls. For the suggested cell, the QE climbs from 80 % to 100 % when wavelength increases from 350 nm to 550 nm. According to fig. 7(b), as the photon energy of the incident light increases, the proposed cell's QE rises to almost 100 % until the photon energy increases from 1.2 eV to 3.5 eV, then gradually falls to reach QE at 85 %. In contrast, for the reference cell, as the photon energy increases from 1.2 eV to 4 eV, the QE initially rises to 90 %, then falls, and after a point becomes constant at 80 % QE.

Jilin Daxue Xuebao (Gongxueban)/Journal of Jilin University (Engineering and Technology Edition)
ISSN：1671-5497
E-Publication Online Open Access
Vol: 41 Issue: 10-2022
DOI 10.17605/OSF.IO/MH3B9

TABLE 8: COMPARISON BETWEEN THE OUTPUT ELECTRICAL PARAMETERS FOR BOTH REFERENCE CELL AND NEW PROPOSED CELL

Solar Cell Structure	V_{oc} *(V)*	J_{sc} *(mA/cm²)*	*FF (%)*	*η (%)*
Reference Cell (p-i-n a-Si:H)	0.97	17.39	69.15	11.62
Optimized Proposed Cell (a-Si:H/SnS/CdS/ZnS)	**1.33**	**36.33**	**87.63**	**42.22**

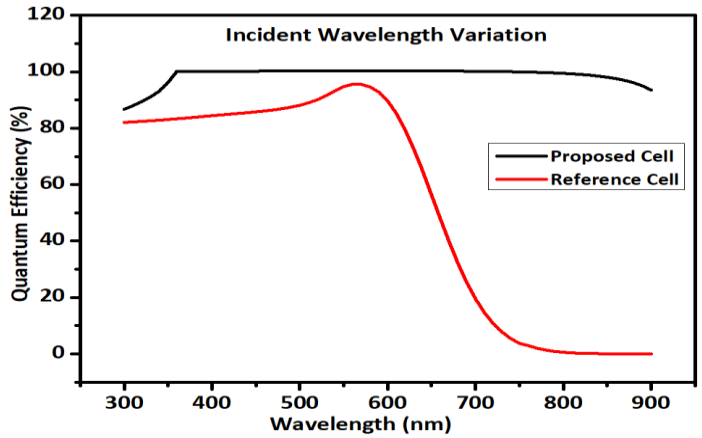

Fig. 7(a): Quantum Efficiency output with Incident Wavelength Variation

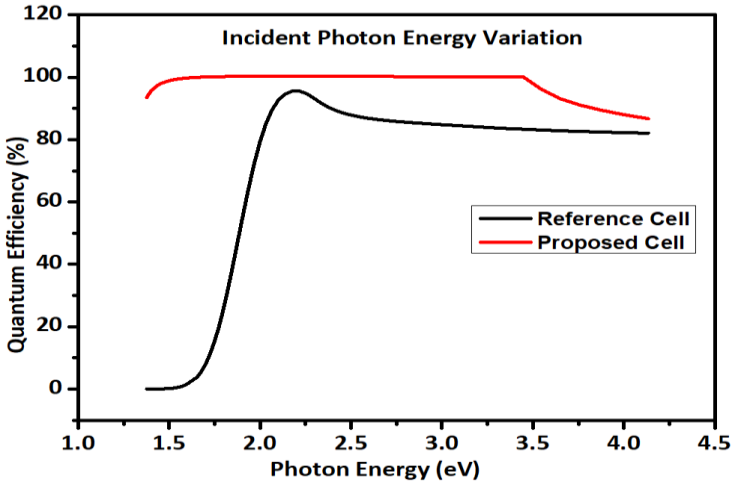

Fig. 7(b): Quantum Efficiency output with Incident Photon Variation

Jilin Daxue Xuebao (Gongxueban)/Journal of Jilin University (Engineering and Technology Edition)
ISSN：1671-5497
E-Publication Online Open Access
Vol: 41 Issue: 10-2022
DOI 10.17605/OSF.IO/MH3B9

5 CONCLUSIONS

On the basis of a numerical analysis performed by the SCAPS (Solar Capacitance Simulator) software programme, a-Si:H based photovoltaic solar cells are compared. The p-i-n a-Si:H, a-Si:H/CdS, a-Si:H/SnS/CdS, a-Si:H/SnS/CdS/ZnS are the cell sequences. After optimization, a new solar cell is finally suggested. SCAPS is given the different input settings for the various levels in order to simulate them. The addition of ZnS to the CdS buffer layer and SnS as a heterojunction layer results in the maximum efficiency. Efficiency declines in the absence of SnS. To emphasise the importance of absorber layer thickness and its function in the device's effectiveness, the absorber layer thickness is simultaneously adjusted. The absorber layers are kept at 1000 nm thick since increasing the thickness of the a-Si:H absorber layer also boosts efficiency. In addition, efficiency declines as operational temperature rises. Efficiency improves compared to the p side, according to illumination variation on the n side. Additionally, bandgap grading is carried out by adjusting the bandgaps of the absorber layer, and the efficiency is raised to 44.89 %. However, a few defects are also added to the real-time scenario solution, which brought the overall efficiency reported in this work down to 42.22 %. It also exhibits superior quantum efficiency over a wider wavelength bandwidth. The ideal solution exhibits an efficiency of 42.22 % at 300 K and AM1.5 lighting at 1000 W/cm^2 which is much higher than the reference cell efficiency of 11.62 %. At a junction of two semiconductor materials, the photovoltaic effect causes charge carriers to be created as a result of photon absorption. The charge carriers are then separated and, finally, accumulated at the junction's terminals.

ACKNOWLEDGMENT

The Department of ELIS at the University of Gent in Belgium and Dr. M. Burgelman and his team are to be thanked for providing unrestricted use of the SCAPS-1D tool.

REFERENCES

[1] H. Shaik and G. M. Rao, “Critical investigation on hydrogen bonding by Fourier Transform Infrared spectroscopy in hydrogenated amorphous silicon thin films,” *J. Non. Cryst. Solids*, vol. 375, pp.88-94, 2013.

[2] H. Shaik and V. Anand, and M. Rao G, “On the quality of hydrogenated amorphous silicon deposited by sputtering,” *Mater. Sci. Semicond. Process.*, vol. 26, no. 1, pp.367-373, 2014.

[3] N. P. Klochko *et al.*, “Development of a new thin film composition for SnS solar cell,” *Sol. Energy*, vol. 134, pp. 156–164, 2016

[4] F. Haque *et al.*, “Growth optimization of ZnS thin films by RF magnetron sputtering as prospective buffer layer in thin film solar cells,” *Chalcogenide Lett.*, vol. 11, no. 4, pp.189-197, 2014.

[5] M. Burgelman, P. Nollet, and S. Degrave, “Modelling polycrystalline semiconductor solar cells,” *Thin Solid Films*, vol. 361, pp. 527–532, 2000.

[6] S. Badyakar and C. Das, “Numerical simulations on a-Si:H/SnS/ZnSe based solar cells,” *Mater. Today Proc.*, vol. 62, pp. 5275–5282, 2022.

ISSN：1671-5497
E-Publication Online Open Access
Vol: 41 Issue: 10-2022
DOI 10.17605/OSF.IO/MH3B9

[7] M. A. Green, E. D. Dunlop, J. Hohl-Ebinger, M. Yoshita, N. Kopidakis, and X. Hao, “Solar cell efficiency tables (Version 58),” *Prog. Photovoltaics Res. Appl.*, vol. 29, no. 7, pp. 657–667, 2021.

[8] M. Burgelman and J. Marlein, “Analysis of graded band gap solar cells with SCAPS,” in *Proceedings of the 23rd European Photovoltaic Solar Energy Conference, Valencia*, pp. 2151–2155, 2008.

[9] F. X. A. Abega, A. T. Ngoupo, and J. M. B. Ndjaka, “Numerical Design of Ultrathin Hydrogenated Amorphous Silicon-Based Solar Cell,” *Int. J. Photoenergy*, vol. 2021, no. Article Id 7506837, pp. 13, 2021.

[10] F. Baig, H. Ullah, Y. H. Khattak, and B. Mari Soucase, “Numerical analysis of SnS Photovoltaic cells,” *Proc. 2016 Int. Renew. Sustain. Energy Conf. IRSEC 2016*, pp. 596–600, 2017.

[11] S. Saha, S. K. Ukil, and M. R. H. Rashed, “Numerical investigation on the performance of new ultra-thin CZTS solar cell using SCAPS,” *3rd Int. Conf. Electr. Inf. Commun. Technol. EICT 2017*, vol. 2018-Janua, no. December, pp. 1–5, 2018.

[12] F. A. Jhuma, M. Z. Shaily, and M. J. Rashid, “Towards high-efficiency CZTS solar cell through buffer layer optimization,” *Mater. Renew. Sustain. Energy*, vol. 8, no. 1, pp.1-7, 2019.